

Porous Carbon derived from Pine Nut Shell prepared by Steam Activation for Supercapacitor Electrode Material

Liyuan Qin¹, Zhiwei Hou¹, Shuang Lu¹, Shuang Liu¹, Zhongyuan Liu¹, Enchen Jiang^{1,2,*}

¹ College of Engineering, Northeast Agricultural University, Harbin, 130025, China

² College of Materials and Energy, South China Agricultural University, Guangzhou, 510642, China

*E-mail: qinliyuan2006@163.com (L. Qin), enchenjiang@hotmail.com (E. Jiang)

Received: 9 April 2019 / Accepted: 27 June 2019 / Published: 31 July 2019

Porous activated carbon (AC) is prepared by the steam activation of biochar prepared from pyrolyzed pine nut shell as a precursor. The effects of various activation temperatures, activation times and steam flow rates on the structure and properties of the obtained ACs are compared and analyzed. The cyclic voltammetry, galvanostatic charge/discharge, electrochemical impedance spectroscopy and cycle stability properties of the ACs are measured in a three-electrode electrochemical system with 6 mol L⁻¹ KOH solution as the electrolyte. The results show that an activation temperature of 850°C, an activation time of 60 min and a steam flow rate of 18 ml h⁻¹ are the optimal conditions. The AC obtained under these conditions displays a specific surface area of 956 m² g⁻¹, a mesopore ratio of 37.1% and a specific capacitance of 128 F g⁻¹ at 0.5 A g⁻¹. Moreover, the AC has a well-developed interconnected hierarchical pore structure including micropores, mesopores and macropores and a good capacitance retention rate of 98% at a current density of 5 A g⁻¹ after 10000 cycles of testing. These high-performance ACs from biomass waste show potential industrial applications in energy storage.

Keywords: pine nut shell; hierarchical porous carbon; steam activation; supercapacitor electrode

1. INTRODUCTION

With the increasing environmental and energy problems around the world, renewable energy has attracted increasing attention [1-2], especially biomass resources, owing to their abundant reserves and multiple species. Pyrolysis technology as a thermochemical method can effectively convert biomass into biochar, bio-oil and non-condensable gas under oxygen-free or oxygen-limited conditions; the reactor is simple and easily controlled [3-4]. As the main product of biomass pyrolysis, biochar has unique physicochemical properties, a fundamental pore structure and a certain adsorption capacity. However, the specific surface area (SSA) of biochar derived from biomass is usually

relatively low, which limits its further application in high-value-added materials, such as carbon-based electrode materials and catalysts [5-6]. The high-value-added utilization of biochar is conducive to enhancing the economy of biomass conversion and biomass energy utilization. Activated carbon (AC) is prepared from biomass with high SSA and controllable pore size with simple preparation processes and low cost. Therefore, converting biochar as a precursor into AC has been considered a good approach. In previous reports, various biomass wastes have been utilized as precursors to obtain AC materials, such as walnut shell using CO₂ as the activating agent [7], waste tea using steam as the activating agent [8], pine wood sawdust using H₃PO₄ as the activating agent [9] and bagasse using KOH as the activating agent [10]. The main methods of preparing AC from biochar are physical activation and chemical activation [11]. Chemical activation has some advantages, such as highly efficient pore development and consequently high SSA. However, physical activation is more environmentally friendly because no chemical reagents are used, reducing the cost of the preparation process as well [7, 12]. Steam is widely used as an activator due to its efficient, clean and safe properties. For example, AC prepared from argan nut shell by steam activation was applied in a high-grade adsorbent [13], and carbon electrodes were derived from corncob residue by a steam activation process [14]. During the steam activation process, the main factors affecting the properties of ACs are the activation temperature, activation time and steam flow rate [15-16].

Pine nut shell (PNS) is one of the main byproducts in the processing of pine nuts, which have a large output every year in China, and the lignin and cellulose content of PNS is approximately 40% [16-17]. Moreover, biochar from PNS (PNSB) has a hard texture, high fixed carbon content and low ash content and is a good precursor material for AC preparation. Effectively utilizing PNS can not only protect the environment but also avoid resource waste. For instance, Chen et al. prepared PNS AC by steam activation, and the highest SSA was 1057.8 m² g⁻¹ with an iodine adsorption value of 958.9 mg g⁻¹ [16]. Deng et al. prepared PNS AC by KOH activation and observed good adsorptive ability for CO₂ at different temperatures and pressures [18]. However, to the best of our knowledge, there is no report on the electrochemical properties of ACs derived from PNS or PNSB used as electrode materials. In this study, PNS was employed as the carbon source, and AC was prepared from PNSB (PAC) by steam activation. The effects of activation temperature, activation time and steam flow rate on the SSA and pore structure of PAC were investigated. In addition, the electrochemical performance of PACs was studied in 6 mol L⁻¹ KOH electrolyte solution. This work aims to provide an approach to prepare AC from PNS as a high-performance electrode material and achieve the high-value-added utilization of biowaste.

2. MATERIAL AND METHODS

2.1 Materials

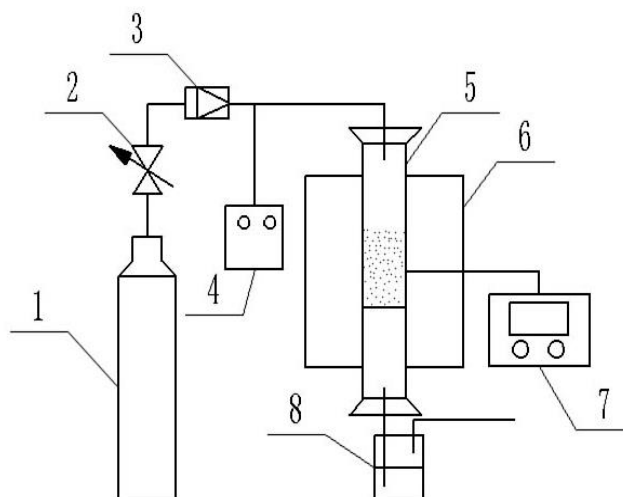
The PNS used as a carbon source was obtained from Heilongjiang Province, China. Before use, the PNS was crushed, passed through 4-6 mm mesh, washed with deionized water and then dried at 75 °C for 24 h. The PNSB was prepared through PNS pyrolysis at a temperature of 500 °C for 15 min.

The component, proximate and elemental analyses of PNS and PNSB are shown in Table 1.

Table 1. Component, proximate and elemental analyses of PNS and PNSB.

	PNS	PNSB
Component analysis (% , dry basis)		
Lignin	38.42	-
Cellulose	33.96	-
Hemicellulose	15.22	-
Proximate analysis (% , dry basis)		
Volatile matter	76.26	21.52
Fixed carbon	23.03	75.77
Ash	0.71	2.71
Elemental analysis (% , dry basis)		
C	47.59	85.93
O	43.74	8.47
H	6.28	2.15
S	1.16	0.57
N	0.56	0.32

2.2 Preparation of PAC



1. Nitrogen cylinder 2.Compression release valve 3. Gas flow indicator 4.Liquid flowmeter 5.Quartz reaction tube 6.Heating electric furnace 7.Digital display temperature controller 8.Exhaust gas treatment

Figure 1. Activation device diagram.

In the activation process, after washing with deionized water, PNSB was dried at 75 °C for 24 h and then crushed to a particle size of 3-5 mm as a precursor material for activation. Each time, 10 g PNSB was placed into the quartz tube of the activation device shown in Fig. 1. After removing the air in the tube by nitrogen, the temperature of the activation device was adjusted to the designated value,

and steam was injected through the pump at a specified flow rate to obtain AC. The selected parameters included activation temperatures of 800, 850 and 900°C, activation times of 45, 60 and 75 min, and steam flow rates of 12, 18 and 24 ml h⁻¹. The AC was washed with deionized water and dried at 85°C for 24 h before use. The prepared ACs from PNSB were denoted as PAC-activation temperature-activation time-steam flow rate, for example, PAC850-60-18. The yield of PAC was calculated using the following equation:

$$Y = \frac{m}{m_0} \times 100\% \quad (1)$$

where Y is the yield of PAC, %; m is the mass of PAC, g; and m_0 is the mass of PNSB, g.

2.3 Characterization of samples

N₂ adsorption/desorption isotherms were measured by a specific surface and aperture analyzer (3H-2000PS1, Bei Shi De Instrument, China). The SSA was obtained by the Brunauer-Emmett-Teller (BET) method. The pore size distribution of mesopores was determined by the Barrett-Joyner-Halenda (BJH) method, and the micropore characteristics were calculated through the t-plot method. The crystal structure and functional groups of samples were detected using X-ray diffraction (XRD, MiniFlex-600, Japan) and Fourier transform infrared spectroscopy (FTIR, Tensor 27, Germany). The morphology of the samples was investigated by scanning electron microscopy (SEM, S-3400, Hitachi, Japan). Elemental analysis was performed on an elemental analyzer (Vario, micro cube, Elementar, Germany).

2.4 Electrochemical measurements

The electrochemical properties were tested in 6 mol L⁻¹ KOH electrolyte using an electrochemical workstation (SP-150, Bio-Logic, France). A platinum electrode and Ag/AgCl electrode were used as the counter electrode and reference electrode, respectively. The working electrodes were fabricated by mixing the prepared AC materials with acetylene black and polytetrafluorethylene (PTFE) in ethanol solution (mass ratio of 8:1:1) and then spreading the slurry onto a piece of nickel foam (1 cm×1 cm). The prepared electrodes were dried at 70°C in a vacuum oven for 12 h and pressed at 10 MPa. Cyclic voltammetry (CV), galvanostatic charge/discharge (GCD), and electrochemical impedance spectroscopy (EIS) were conducted at a voltage range from -1.1 to -0.1 V. The frequency of the EIS test ranged from 10⁻² to 10⁻⁵ Hz. The specific capacitance of the AC samples was calculated from the GCD curves using the following equation [19-20]:

$$C_s = I \times \frac{\Delta t}{m \times \Delta V} \quad (2)$$

where C_s is the specific capacitance, F g⁻¹; I is the current density, A g⁻¹; Δt is the discharge time, s; m is the mass of active material, g; and ΔV is the range of voltage, V.

3. RESULTS AND DISCUSSION

The porosity of PAC was characterized by N_2 adsorption-desorption tests at 77 K, and the results are shown in Fig. 2. The characteristic pore parameters of PAC are summarized in Table 2. Fig. 2(a) shows the N_2 adsorption-desorption isotherms of PAC obtained under different conditions. According to the IUPAC classification, all the PAC samples exhibit type I isotherms. The adsorption values sharply increase at a relative pressure $P/P_0 < 0.1$, indicating the existence of a large number of microporous in the prepared PACs. Furthermore, when the relative pressure $P/P_0 > 0.1$, the adsorption values increase slowly, and a hysteresis loop is observed at a relative pressure $P/P_0 > 0.4$, which suggests the existence of mesoporous in the PAC structure. Among the PAC samples, the adsorption volume of PAC850-60-18 is the largest, and its hysteresis loop is more pronounced, which is characteristic of microporous materials with higher amounts of mesopores. The pore size distributions of PACs obtained under different activation conditions are shown in Fig. 2(b), which shows that the micropore and mesopore size of the PACs are concentrated at 0.5-0.8 nm and 2-4 nm, respectively, which verifies the coexistence of microporous and mesoporous.

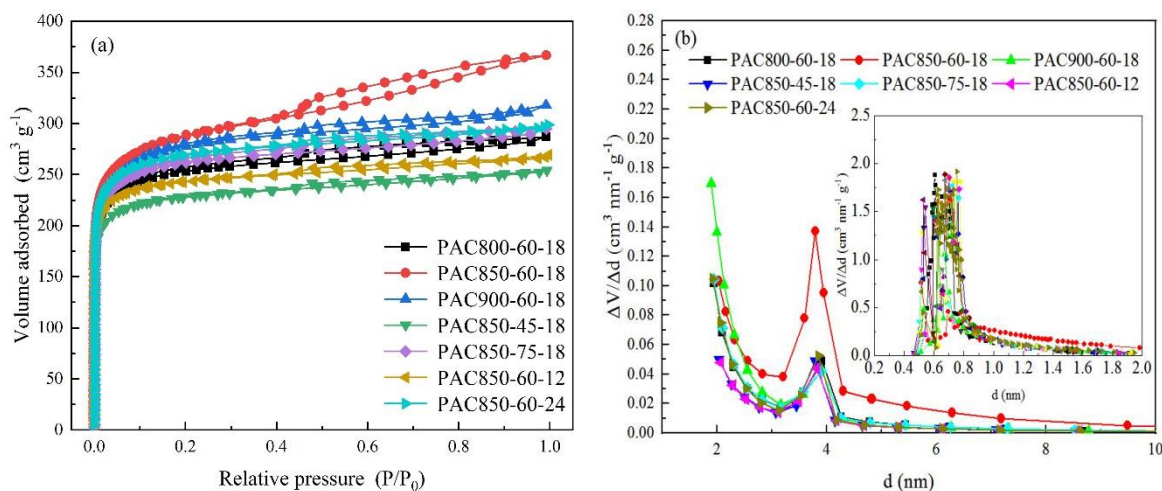


Figure 2. (a) Nitrogen adsorption-desorption isotherms and (b) mesopore pore size distribution of PAC (the inset shows the pore size distribution of the micropore).

As seen from the data in Table 2, the yields of the prepared PACs range from 25.2% to 49.2% under various activation conditions. As the activation temperature, activation time and steam flow rate increase during the activation process, the SSA, total pore volume, micropore volume and mesopore volume of PACs all increase at first and then decrease, while the yield of PAC gradually decreases. This is because a higher activation temperature, activation time and steam flow rate can promote the reaction between PNSB and steam, which increases desorption, distillation and the removal of volatile compounds and forms a large number of micropores, mesopores and even macropores in the PAC. However, as the activation parameters increase further, the reaction between PNSB and steam becomes more intense, which causes some of the existing micropores to be transformed into mesopores or

macropores, and mesopores and macropores collapse. In addition, the excess steam flow causes a temperature decrease on the PNSB surface and weakens the activation reaction. Thus, the SSA, total pore volume, micropore volume and mesopore volume of all PACs are decreased. A higher SSA and mesopore ratio in the prepared PACs are advantageous for charge storage and ion diffusion, leading to excellent capacitance performance [21-22]. PAC850-60-18 shows the largest SSA of $956 \text{ m}^2 \text{ g}^{-1}$, the highest total pore volume of $0.62 \text{ cm}^3 \text{ g}^{-1}$ with a mesopore ratio of 37.1% and an appropriate yield of 36.2%.

Table 2. Summary of the porosity parameters of PAC.

Sample	Yield %	S_{BET}^a $\text{m}^2 \text{ g}^{-1}$	V_t^b $\text{cm}^3 \text{ g}^{-1}$	V_{mic}^c $\text{cm}^3 \text{ g}^{-1}$	V_{mes}^d $\text{cm}^3 \text{ g}^{-1}$	V_{mes}/V_t^e %	D^f nm
PAC800-60-18	37.5	803	0.44	0.37	0.07	15.9	2.21
PAC850-60-18	36.2	956	0.62	0.39	0.23	37.1	2.59
PAC900-60-18	25.2	889	0.49	0.38	0.11	22.4	2.21
PAC850-45-18	49.2	705	0.40	0.33	0.07	17.5	2.26
PAC850-75-18	30.6	812	0.48	0.37	0.11	22.9	2.27
PAC850-60-12	47.4	760	0.42	0.36	0.06	14.3	2.21
PAC850-60-24	29.3	841	0.46	0.39	0.07	15.2	2.22

^a SSA determined according to BET. ^b Total pore volume. ^c Micropore volume. ^d Mesopore volume.

^e Mesopore ratio. ^f Average pore diameter.

Fig. 3 shows the surface morphology of PAC850-60-18. From the low-magnification image in Fig. 3(a), it can be seen that after activation, PAC850-60-18 shows an abundant pore structure and not only maintains a large number of micropores and greater number of mesopores as mentioned above but also develops many macropores. Therefore, the prepared PAC is a typical hierarchical porous structure with regular circular-shaped features including microporous, mesoporous and macroporous. The uniform porous structure is more clearly seen in the high-magnification image in Fig. 3(b); this structure formed because there is no chemical corrosion in steam activation. The reactions are as follows: $\text{C} + \text{H}_2\text{O} \rightarrow \text{H}_2 + \text{CO}$; $\text{C} + \text{H}_2\text{O} \rightarrow \text{H}_2 + \text{CO}_2$; $\text{C} + \text{H}_2 \rightarrow \text{CH}_4$; $\text{C} + \text{CO}_2 \rightarrow \text{CO}$ [23]. These connected pores are beneficial for the rapid migration and diffusion of electrolyte ions in the pore channels of carbon materials.

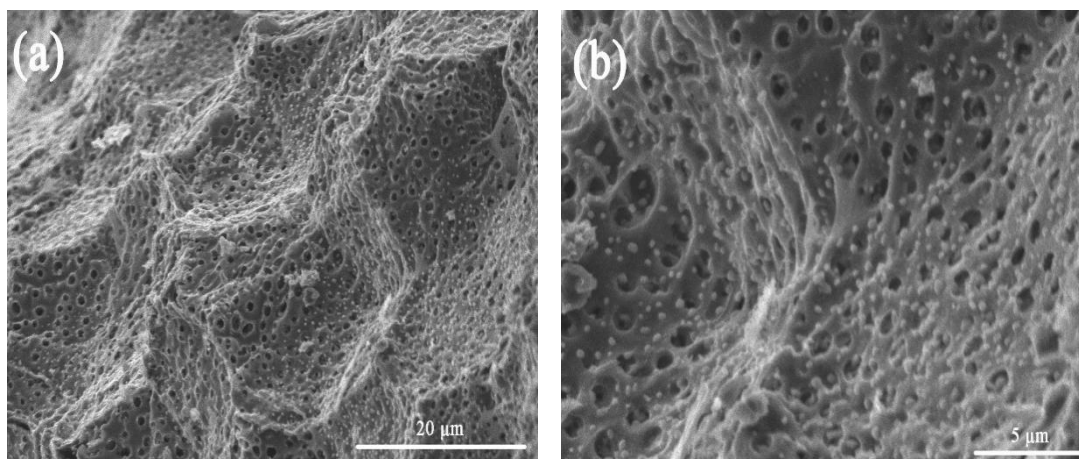


Figure 3. SEM images of PAC850-60-18: (a) low-magnification image; (b) high-magnification image.

Compared with PNSB, the crystallinity and functional groups of PAC850-60-18 were analyzed by XRD and FTIR, and the results are shown in Fig. 4. The XRD patterns in Fig. 4(a) show that PAC850-60-18 and PNSB both have (002) and (100) diffraction peaks at 23° and 43° , respectively, which are typical amorphous structures. The peak intensity of PAC850-60-18 is slightly higher, indicating that activation can enhance the graphitization degree [24-25]. Because the carbon atoms can realign a more stable structure in the activation process and form a more obvious graphitization structure.

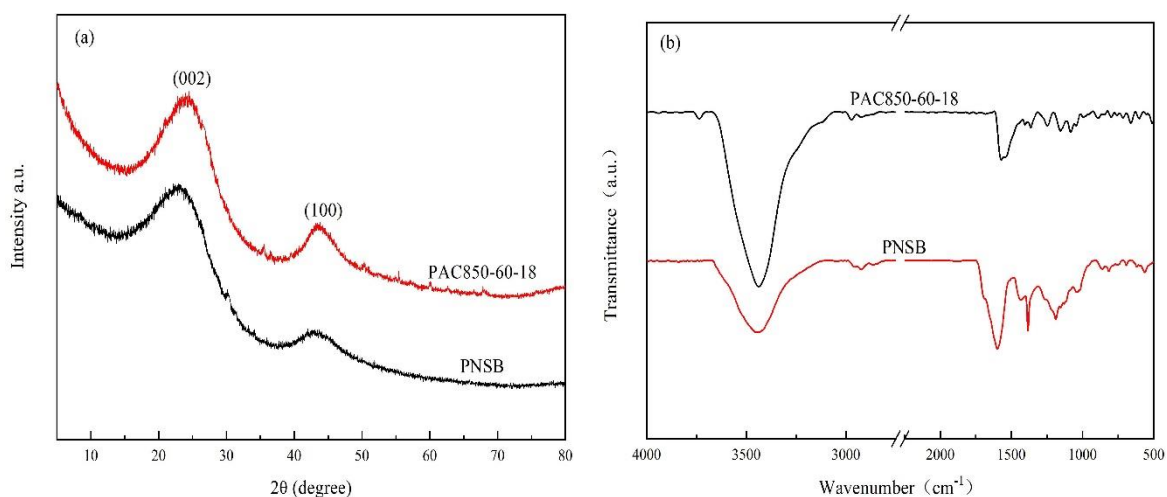
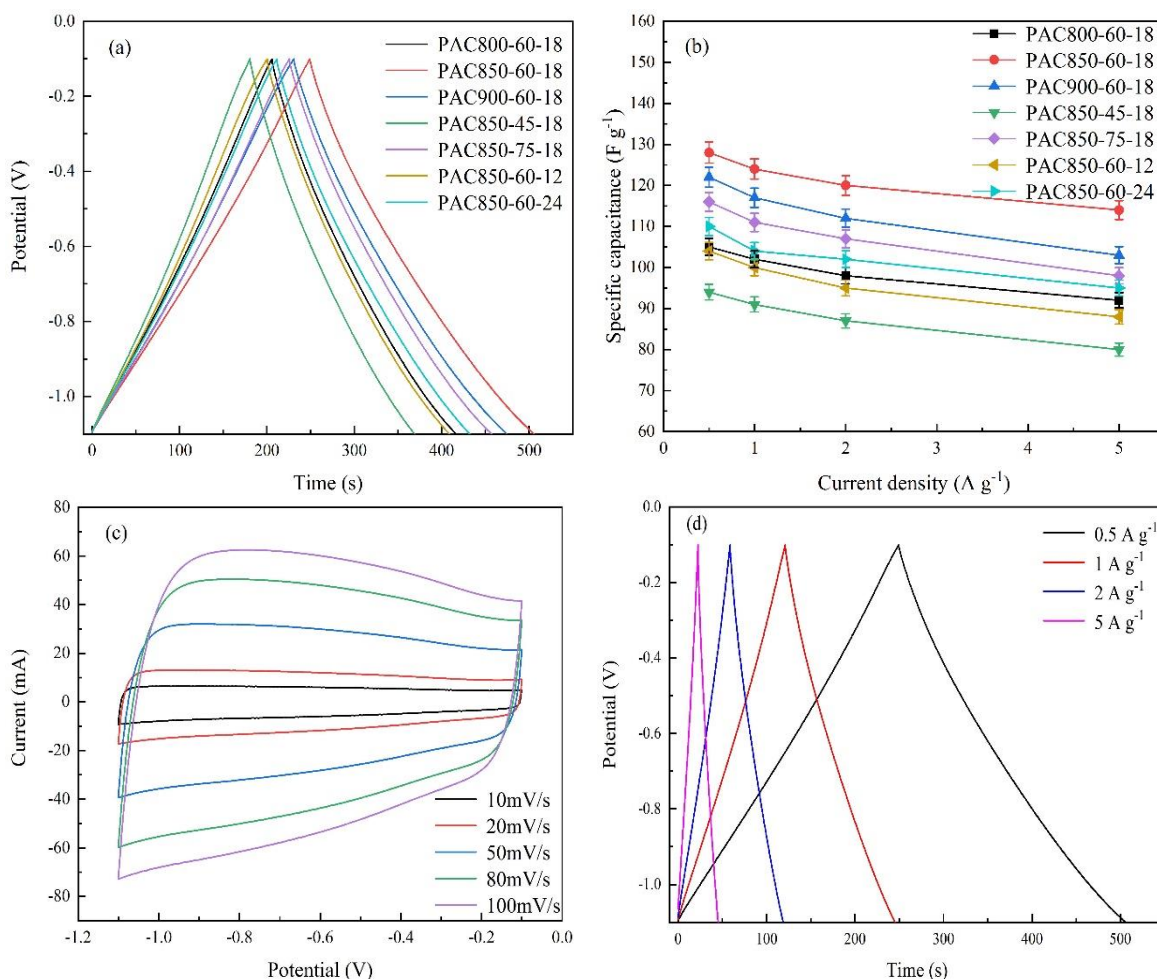


Figure 4. (a) XRD patterns and (b) FTIR spectra of PNSB and PAC850-60-18.

Moreover, there is an up-turned tail in the PAC850-60-18 pattern from 5° to 10° , indicating that there are many nanoporous in the PAC850-60-18 structure [26]. The FTIR spectra of PNSB and PAC850-60-18 are presented in Fig. 4(b), and both spectra are similar. The sharp peak at 3440 cm^{-1} is assigned to the stretching vibration of O-H, indicating the presence of hydroxyl groups; the peaks from 1450 cm^{-1} to 1650 cm^{-1} correspond to C=C in olefins or aromatic compounds. However, some

absorption peaks of PAC850-60-18 are weak and even disappear from 650 to 1275 cm^{-1} , which indicates that some organic compounds associated with the functional groups of C-O, C-H and aromatic compounds in PNSB may decompose in the process of high-temperature activation [27-28]. Although some functional groups disappear, hydrophilic oxygen functional groups such as carboxyl, hydroxyl and carbonyl are retained in PAC850-60-18; such groups can improve the wettability of carbon materials.

The electrochemical performances of the prepared PAC were evaluated, and the results are shown in Fig. 5. The GCD curves of the PACs prepared under different activation conditions at a current density of 0.5 A g^{-1} are shown in Fig. 5(a). All PACs show linear and symmetrical profiles, suggesting good reversible and ideal capacitive behavior for supercapacitor electrode materials [29]. Among these PACs, PAC850-60-18 indicates the optimal capacitive performance with the longest discharge time. According to equation (2), the specific capacitance of PACs was calculated and is shown in Fig. 5(b). PAC850-60-18 shows the largest specific capacitance, 128 A g^{-1} at 0.5 A g^{-1} and 114 A g^{-1} at 5 A g^{-1} . When the current density increases by 10-fold, the capacitance of PAC850-60-18 decreases but remains at 89.1%, which indicates good rate performance. The highest specific capacitance of PAC850-60-18 is ascribed to the higher SSA, total pore volume and mesopore ratio. The other prepared PACs show a similar change trend: the specific capacitance decreases with increasing current density.



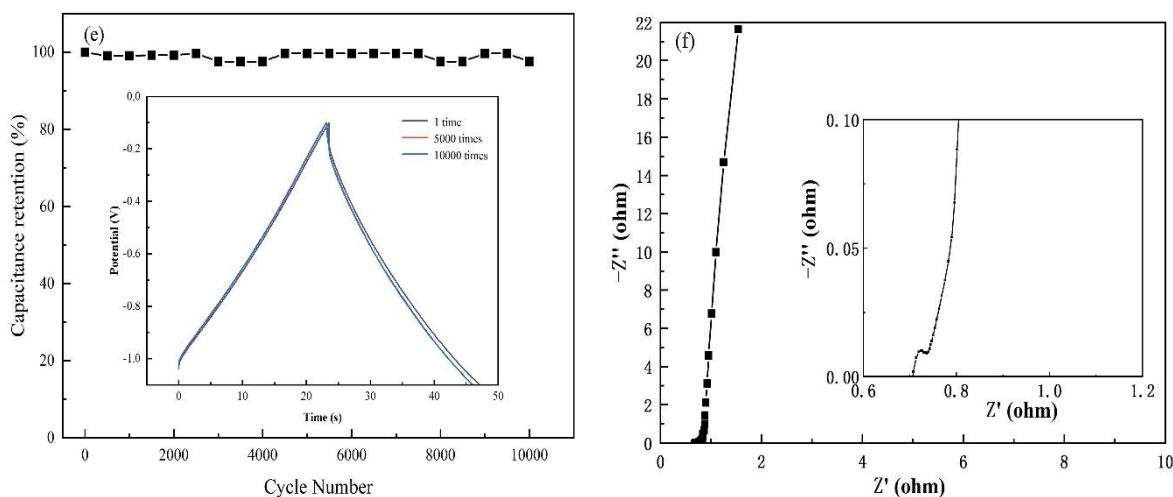


Figure 5. Electrochemical properties of PAC in 6 M KOH: (a) GCD curves of PAC at a current density of 0.5 A g^{-1} ; (b) Specific capacitance of the PAC electrode at different current densities. (c) CV curves of PAC850-60-18 at different scanning rates; (d) GCD curves of PAC850-60-18 at different current densities; (e) cyclic curve (the inset shows GCD curves with different cycles) and (f) Nyquist plots (the inset shows the high-magnification plot of the high-frequency region).

In hierarchical porous carbon electrode materials, abundant micropores provide more adsorption sites for charge storage, and well-developed mesopore and macropore structures act as channels for electrolyte ion transfer and provide easy access to the micropores of carbon electrodes [21, 30]. Therefore, the best performance of PAC850-60-18 can be expected, which is consistent with the adsorption-desorption test analysis.

Fig. 5(c) shows the CV curves of PAC850-60-18 at scan rates from 10 mV/s to 100 mV/s . The CV curves indicate a typical nearly rectangular shape, and no dramatic distortion is observed even at 100 mV/s , which suggests an ideal capability for use as a supercapacitor electrode material. Furthermore, there is no weak redox peak in the CV curves, indicating no pseudocapacitance in the AC/electrolyte system, and the specific capacitance is almost entirely supplied by double layers [31-33]. GCD curves of PAC850-60-18 from a current density of 0.5 A g^{-1} to 5 A g^{-1} are shown in Fig. 5 (d). Although the charge-discharge time of PAC850-60-18 decreases obviously with increasing current density, all the curves show an approximately symmetric triangle shape. In addition, Fig. 5(e) shows that PAC850-60-18 has a 98% capacitance retention rate after 10000 charge-discharge cycles at a current density of 5 A g^{-1} , which indicates excellent cycling stability. Further confirmation of the excellent cycling stability is shown in the inset of Fig. 5(e) by comparing the 1st and 10000th cycle curves. The Nyquist plot of PAC850-60-18 is shown in Fig. 5(f). The plot shows a semicircle in the high-frequency region corresponding to the interfacial charge transfer resistance at the electrode/electrolyte interface and a vertical line in the low-frequency region, which is related to the uniform pore size distribution of carbon materials [34-36]. The equivalent series resistance (ESR) of PAC850-60-18, calculated by the intercept between the curve and the real axis, is approximately 0.72Ω , which is relatively small. In addition, PAC850-60-18 shows a line that more closely approximates a straight line perpendicular to the horizontal axis in the low-frequency region. Therefore, AC derived from PNS with a hierarchical pore structure is a feasible double-layer capacitance electrode material

with excellent cycling stability under high current density (Fig. 5 (e)).

The PAC in this work was compared with other high-quality ACs derived from biomass waste in previous studies, and the characteristic parameters are summarized in Table 3. ACs prepared through steam activation usually show micropore-dominated structures with large SSA and are usually used as adsorbents due to their good adsorption capacity [13, 37]. However, the coexistence of hierarchical microporous and mesoporous/macroporous structure usually benefits capacitive properties and is more suitable for application as an electrode material [34]. Although the SSA of ACs that only have microporous and mesoporous in their structure is higher [14, 38-39], the specific capacitance and cyclic stability of the ACs with a hierarchical structure of microporous, mesoporous and macroporous in this work is much better. The PAC850-60-18 in this work, prepared by pyrolysis combined with steam activation, showed a specific capacitance of 128 F g⁻¹ at 0.5 A g⁻¹, which approaches that of ACs with the same structure prepared by KOH activation [10]. Moreover, PAC850-60-18 exhibits a better capacitance retention rate of 98% at 5 A g⁻¹ after 10000 cycles than that of AC prepared by KOH activation [10, 39] due to the higher mesopore ratio of 37.1%. The low-cost PAC in this study shows excellent performance and a simple and environmentally friendly preparation method. Therefore, this approach can provide a good method for the preparation and utilization of high-quality AC from PNS biomass waste.

Table 3. Comparison of the PAC obtained in this work with materials in the literature.

Biomass precursor	Activation method	Pore structure	S_{BET} m ² g ⁻¹	Adsorption efficiency mg g ⁻¹	Specific capacitance F g ⁻¹	Cyclic stability %	Ref.
Argan nut shell	Steam	Microporous	2853	1408 (Bisphenol A)	-	-	[13]
Corn cob	Steam	Microporous	980	665.23 (Iodine)	-	-	[37]
Corn cob residue	Steam	Micro/mesoporous	1210	-	120/1 A g ⁻¹	100/1 A g ⁻¹ (5000 times)	[14]
Oil palm kernel shell	Steam	Micro/mesoporous	727.3	-	123/0.5 A g ⁻¹	97/5 A g ⁻¹ (1000 times)	[38]
Cow dung	KOH	Micro/mesoporous	1984	-	117/1 A g ⁻¹	85/1 A g ⁻¹ (1000 times)	[39]
Bagasse	KOH	Micro/meso/macroporous	1892.4	-	142.1/0.5 A g ⁻¹	93.9/1 A g ⁻¹ (5000 times)	[10]
Pine nut shell	Steam	Micro/meso/macroporous	921	-	128/0.5 A g ⁻¹ 124/1 A g ⁻¹	98/5 A g ⁻¹ (10000 times)	This work

4. CONCLUSION

Porous activated carbon derived from biomass waste (PNS) was prepared by eco-friendly steam activation combined with continuous pyrolysis. The PAC has well-developed interconnected hierarchical pore structures consisting of microporous, mesoporous and macroporous, which shorten the pathway of electrolyte ion transportation. PAC obtained under activation conditions of 850 °C, 60 min and a steam flow rate of 18 ml h⁻¹ demonstrated a relatively high SSA of 956 m² g⁻¹ and good electrochemical performance with a specific capacitance of 128 F g⁻¹ at 0.5 A g⁻¹ and maintained 114 F g⁻¹ at 5 A g⁻¹ with a capacitance retention rate of 89.1%. After 10000 cycles of testing, the capacitance retention rate of the PAC was maintained at 98% at a current density of 5 A g⁻¹, suggesting good rate capability. A facile approach for high-value-added conversion and application of PNS as an electrode material has been demonstrated.

ACKNOWLEDGEMENTS

The research work was supported by the University Nursing Program for Young Scholars with Creative Talents in Heilongjiang Province (UNPYSCT-2017001)

References

1. J. Popp, Z. Lakner, M. Harangi-Rókos and M. Fári, *Renewable Sustainable Energy Rev.*, 32 (2014) 559.
2. Y. Li, S. Zhao, K. Tagawa and F. Feng, *Energy Convers. Manage.*, 167 (2018) 70.
3. V. Dhyani and T. Bhaskar, *Renewable Energy*, 129 (2018) 695.
4. D. Vamvuka, S. Sfakiotakis and O. Pantelaki, *Fuel*, 236 (2019) 574.
5. A. M. Abioye and F. N. Ani, *Renewable Sustainable Energy Rev.*, 52 (2015) 1282.
6. L. Yang, F. Liu, Y. Liu, W. Quan and J. He, *Int. J. Hydrogen Energy*, 43 (2018) 17633.
7. J. Zhou, A. Luo and Y. Zhao, *J. Air Waste Manage. Assoc.*, 68 (2018) 1269.
8. Y. Sun, H. Li, G. Li, B. Gao, Q. Yue and X. Li, *Bioresour. Technol.*, 217 (2016) 239.
9. X. Gao, L. Wu, Z. Li, Q. Xu, W. Tian and R. Wang, *J. Mater. Cycles Waste Manage.*, 2 (2018) 925.
10. D. Yang, H. Jing, Z. Wang, J. Li, M. Hu, R. Lv, R. Zhang and D. Chen, *J. Colloid Interface Sci.*, 528 (2018) 208.
11. L. Wu, Z. Shang, H. Wang, W. Wan, X. Gao, Z. Li and N. Kobayashi, *J. Mater. Cycles Waste Manage.*, 20 (2018) 1676.
12. P. N. Y. Yek, R. K. Liew, M. S. Osman, C. L. Lee, J. H. Chuah, Y. Park and S. S. Lam, *J. Environ. Manage.*, 236 (2019) 245.
13. M. Zbair, K. Ainassaari, Z. E. Assal, S. Ojala, N. E. Ouahedy, R. L. Keiski, M. Bensitel and R. Brahmi, *Environ. Sci. Pollut. Res.*, 25 (2018) 35657.
14. W. Qu, Y. Xu, A. Lu, X. Zhang and W. Li, *Bioresour. Technol.*, 189 (2015) 285.
15. M. Sivachidambaram, J. J. Vijaya, K. Niketha, L. J. Kennedy, E. Elanthamilan and J. P. Merlin, *J. Nanosci. Nanotechnol.*, 19 (2019) 3388.
16. D. Chen, X. Chen, J. Sun, Z. Zheng and K. Fu, *Bioresour. Technol.*, 216 (2016) 629.
17. S. Uçar and S. Karagöz, *Fuel*, 137 (2014) 85.
18. S. Deng, H. Wei, T. Chen, B. Wang, J. Huang and G. Yu, *Chem. Eng. J.*, 253 (2014) 46.
19. T. Jiang, Q. Sun, W. Xu, G. Zhao and J. Shi, *Int. J. Electrochem. Sci.*, 13 (2018) 11480.
20. H. Tenmyo, R. Sugihara, A. Ohta, T. Asano, T. Uematsu, T. Tsuda, J. Maruyama, S. Iwasaki, H. Uyama and S. Kuwabata, *Electrochemistry*, 87 (2019) 119.

21. J. Yang, H. Wu, M. Zhu, W. Ren, Y. Lin, H. Chen and F. Pan, *Nano Energy*, 33 (2017) 453.
22. H. Feng, H. Hu, H. Dong, Y. Xiao, Y. Cai, B. Lei, Y. Liu and M. Zheng, *J. Power Sources*, 302 (2016) 164.
23. M. G. Plaza, A. S. González, J. J. Pis, F. Rubiera and C. Pevida, *Appl. Energy*, 114 (2014) 551.
24. Y. Wu, J. P. Cao, X. Y. Zhao, Z. Q. Hao, Q. Q. Zhuang, J. S. Zhu, X. Y. Wang and X. Y. Wei, *Electrochim. Acta*, 252 (2017) 397.
25. C. Xu, F. Xu, L. Sun, L. Cao, F. Yu, H. Zhang, E. Yan, H. Peng, H. Chu and Y. Zou, *Int. J. Electrochem. Sci.*, 14 (2019) 1782.
26. Z. Li, L. Zhang, X. Chen, B. Li, H. Wang and Q. Li, *Electrochim. Acta*, 296 (2019) 8.
27. W. Tongpoothorn, M. Sriuttha, P. Homchan, S. Chanthai and C. Ruangviriyachai, *Chem. Eng. Res. Des.*, 89 (2011) 335.
28. N. Ozbay and A. S. Yargic, *J. Appl. Polym. Sci.*, 136 (2019) 47185.
29. N. Zhao, L. Deng, D. Luo, S. He and P. Zhang, *Int. J. Electrochem. Sci.*, 13 (2018) 10626.
30. D. Zhu, Y. Wang, W. Lu, H. Zhang, Z. Song, D. Luo, L. Gan, M. Liu and D. Sun, *Carbon*, 111 (2017) 667.
31. X. Tian, H. Ma, Z. Li, S. Yan, L. Ma, F. Yu, G. Wang, X. Guo, Y. Ma and C. Wong, *J. Power Sources*, 359 (2017) 88.
32. L. Z. Fan, S. Qiao, W. Song, M. Wu, X. He and X. Qu, *Electrochim. Acta*, 105 (2013) 299.
33. H. Tenmyo, T. Asano, Y. Jo, K. Yoshii, T. Tsuda, J. Maruyama, H. Uyama and S. Kuwabata, *Electrochemistry*, 83 (2015) 348.
34. Y. Gao, W. Zhang, Q. Yue, B. Gao, Y. Sun, J. Kong and P. Zhao, *J. Power Sources*, 270 (2014) 403.
35. H. Que, C. Chang, X. Yang, F. Jiang and M. Li, *Int. J. Electrochem. Sci.*, 14 (2019) 3477.
36. B. Niu, M. Yuan, F. Jiang and M. Li, *Int. J. Electrochem. Sci.*, 14 (2019) 3253.
37. M. Song, B. Jin, R. Xiao, L. Yang, Y. Wu, Z. Zhong and Y. Huang, *Biomass Bioenergy*, 48 (2013) 250.
38. I. I. Misnon, N. K. M. Zain, R. A. Aziz, B. Vidyadharan and R. Jose, *Electrochim. Acta*, 174 (2015) 78.
39. D. Bhattacharjya and J. Yu, *J. Power Sources*, 262 (2014) 224.

© 2019 The Authors. Published by ESG (www.electrochemsci.org). This article is an open access article distributed under the terms and conditions of the Creative Commons Attribution license (<http://creativecommons.org/licenses/by/4.0/>).